Explicit calculations of Wet Bulb Globe Temperature compared with approximations and why it matters for labor productivity

Qinqin Kong[1] and Matthew Huber[1]

[1]Purdue University

November 23, 2022

Abstract

Wet bulb globe temperature (WBGT) is a widely applied heat stress index. However, most applications of WBGT within the heat stress impacts literature do not use WBGT at all, but one of the ad hoc approximations, typically the simplified WBGT (sWBGT) or the environmental stress index (ESI). Surprisingly little is known about how well these approximations work for the global climate and climate change settings that they are being applied to. Here we assess the bias distribution as a function of temperature, humidity, wind speed and radiative conditions of both sWBGT and ESI relative to a well-validated, explicit physical model for WBGT developed by Liljegren, within an idealized context and the more realistic setting of ERA5 reanalysis data. sWBGT greatly overestimates heat stress in hot-humid areas. ESI has much smaller biases in the range of standard climatological conditions. However, both metrics may substantially underestimate extreme heat especially over subtropical dry regions. These systematic biases demonstrate that sWBGT-derived estimates of heat stress and its health and labor consequences are significantly overestimated over much of the world today. We recommend discontinuing the use of sWBGT. ESI may be acceptable for assessing average heat stress or integrated impact over a long period like a year, but less suitable for health applications, extreme heat stress analysis, or as an operational index for heat warning, heatwave forecasting or guiding activity modification at workplace. Nevertheless, Liljegren's approach should be preferred over these ad hoc approximations and we provide a Python implementation to encourage its widespread use.

Explicit calculations of Wet Bulb Globe Temperature compared with approximations and why it matters for labor productivity

Qinqin Kong[1] **and Matthew Huber**[1]

[1]Department of Earth, Atmospheric, and Planetary Sciences, Purdue University, West Lafayette, United States of America, 47907

Key Points:

- Most climate change heat stress impacts studies which claim to use WBGT, employ instead ad hoc approximations.
- We evaluate the biases of two commonly used approximations within both an idealized and the more realistic setting of ERA5 reanalysis data.
- We provide an accessible and computationally efficient Python implementation to facilitate widespread uptake of accurate WBGT calculations.

Corresponding author: Qinqin Kong, `kong97@purdue.edu`

Abstract

Wet bulb globe temperature (WBGT) is a widely applied heat stress index. However, most applications of WBGT within the heat stress impacts literature do not use WBGT at all, but one of the ad hoc approximations, typically the simplified WBGT (sWBGT) or the environmental stress index (ESI). Surprisingly little is known about how well these approximations work for the global climate and climate change settings that they are being applied to. Here we assess the bias distribution as a function of temperature, humidity, wind speed and radiative conditions of both sWBGT and ESI relative to a well-validated, explicit physical model for WBGT developed by Liljegren, within an idealized context and the more realistic setting of ERA5 reanalysis data. sWBGT greatly overestimates heat stress in hot-humid areas. ESI has much smaller biases in the range of standard climatological conditions. However, both metrics may substantially underestimate extreme heat especially over subtropical dry regions. These systematic biases demonstrate that sWBGT-derived estimates of heat stress and its health and labor consequences are significantly overestimated over much of the world today. We recommend discontinuing the use of sWBGT. ESI may be acceptable for assessing average heat stress or integrated impact over a long period like a year, but less suitable for health applications, extreme heat stress analysis, or as an operational index for heat warning, heatwave forecasting or guiding activity modification at workplace. Nevertheless, Liljegrens approach should be preferred over these ad hoc approximations and we provide a Python implementation to encourage its widespread use.

Plain Language Summary

Wet bulb globe temperature (WBGT) is a widely applied heat stress index. However, most applications of WBGT within the climate change heat stress impacts literature do not use WBGT at all, but one of the ad hoc approximations, typically the simplified WBGT (sWBGT) or sometimes the environmental stress index (ESI). But we know little about how well these approximations work for measuring heat stress. Here we evaluate the performance of sWBGT and ESI against a well-validated, explicit physical model of WBGT. sWBGT greatly overestimates heat stress under hot, humid climate. ESI performs much better in measuring average heat stress. But they both may seriously underestimate severe heat stress especially in hot, dry regions. Our results suggest that previous estimates of heat stress and its impact using sWBGT tend to be largely overestimated. We recommend discontinuing the use of sWBGT. ESI may be acceptable for assessing average heat stress, but less suitable for the warning or forecasting of extreme heat, or providing guidance for employees and employers to deal with heat stress at workplace. Nevertheless, the well-validated physical model of WBGT should be preferred over these approximations and we provide a Python implementation to encourage its more widespread use.

1 Introduction

Heat stress has caused more deaths than any other extreme weather event, and is recognized to have broad social and economic impacts such as heat-related illness (Barriopedro et al., 2011; Mora et al., 2017; Ebi et al., 2021), conflict (Burke et al., 2009; Schleussner et al., 2016), crime (Shen et al., 2020), electricity demand(Maia-Silva et al., 2020), and labor productivity reduction (Dunne et al., 2013; Kjellstrom et al., 2016; Masuda et al., 2021; Orlov et al., 2020; Hsiang et al., 2017). Heat stress will become a even bigger threat in the future as the world warms (Diffenbaugh & Giorgi, 2012; Meehl & Tebaldi, 2004; Willett & Sherwood, 2010; Sherwood & Huber, 2010; D. Li et al., 2020).

As well reviewed elsewhere, many heat stress metrics have been developed (de Freitas & Grigorieva, 2014; Epstein & Moran, 2006; Havenith & Fiala, 2015). Among these the wet bulb globe temperature (WBGT) is arguably the most popular one, enjoying the advantages of a simple physical interpretation, covering all four ambient factors (temperature, humidity, wind and radiation) contributing to heat stress, and having well established safety thresholds to guide activity modification within the military (Army, 2003), occupational (NIOSH, 2016) and athletic settings (ACSM, 1984). It is constructed as a linear combination of natural wet bulb temperature (T_w), black globe temperature (T_g) and dry bulb temperature (T_a): $WBGT = 0.7T_w + 0.2T_g + 0.1T_a$ (Yaglou & Minard, 1957).

Measurement of WBGT requires costly instrument and time-consuming attention by experienced operators which prevents it to become a routine meteorological measurement at weather stations. As a result, several approaches have been developed to approximate WBGT, with the simplified WBGT (sWBGT) (ABM, 2010) and environmental stress index (ESI) (D. Moran et al., 2001; D. Moran, Pandolf, Laor, et al., 2003) being representative of many similar ad hoc approaches.

sWBGT (ABM, 2010) is an approximate form requiring only temperature and humidity and explicitly assuming fixed moderately high solar radiation and low wind speeds which implies potential positive or negative biases when these assumptions are not met. It has been widely used because of its simplicity for assessing heat stress and the implication on athletes and labor (Smith et al., 2018; Willett & Sherwood, 2010; Kakamu et al., 2017; Cooper et al., 2016; Lee & Min, 2018; Zhu et al., 2021; Kjellstrom et al., 2009; Liu, 2020; Altinsoy & Yildirim, 2014). ESI was constructed via a multiple regression with WBGT being the dependent variable and temperature, humidity, solar radiation and their interaction terms being independent variables (D. Moran et al., 2001). ESI was validated across different climate regimes over Israel and New Zealand based on large databases (D. Moran, Pandolf, Shapiro, et al., 2003; D. Moran et al., 2004; D. S. Moran et al., 2004, 2005). Although a high correlation (>0.9) between WBGT and ESI was achieved, the residual errors can be up to ±2°C, and it may be the critical situations (such as extreme heat stress) where ESI substantially under- or overestimate WBGT (Havenith & Fiala, 2015).

Outside of the limited conditions for which these approximate forms were developed, little is known about how well these approximations work for the global climate and climate change settings that they are being applied to. Although a few studies had quantified biases of sWBGT or ESI based on local meteorological measurements (D. Moran et al., 2004; D. S. Moran et al., 2004, 2005; Grundstein & Cooper, 2018), the results are not readily transferable to other regions with different climate conditions. A recent study employed both sWBGT and ESI to assess labor reduction due to intensifying heat stress, and found vast differences between the two metrics (de Lima et al., 2021). However, it is not clear which one is more close to the reality. Given the expected biases of both metrics, and their large discrepancies in indicating labor loss, it is necessary to assess the magnitude of these biases and the consequent influences on heat stress impact assessment, which is crucial for determining the suitability of each metric under certain application scenarios.

Aside from the simple approximations of WBGT described above, physical models on the energy balance of WBGT sensors have also been developed which enable a direct simulation of WBGT measurements from weather station observations or climate model output (Gaspar & Quintela, 2009; C. H. Hunter & Minyard, 1999; Bernard & Pourmoghani, 1999; Liljegren et al., 2008; Dernedde & Gilbert, 1991). Among them, the model developed by Liljegren et al. (2008) is a highly sophisticated one being well calibrated and validated (with a RMS difference of less than 1°C) (Liljegren et al., 2008; Lemke & Kjellstrom, 2012). However, Liljegren's approach has seen limited applications (Takakura et al., 2017, 2018; Casanueva et al., 2020; Jacobs et al., 2019; Orlov et al., 2019) potentially because it is complex and computationally intensive. Moreover, Liljegren's code was written in C and FORTRAN language which may be not familiar to most end-users.

To resolve this issue, we rewrote the code in Cython which is fast, easy to use in Python, and scales well for large dataset such as climate model output.

Here we treat Liljegren's model as a ground truth, and explores the bias distributions of sWBGT and ESI within both an idealized context and the more realistic setting of ERA5 reanalysis data. The paper is structured as follows. Section 2 introduces more details on the metrics and Liljegren's model, as well as data source and analysis methods. Section 3 presents bias quantification results including first the bias distribution within an idealized context as a function of temperature, humidity, wind speed and radiative conditions, and second the error structure introduced within ERA5 reanalysis data. In section 4, the potential consequences of these biases are examined through an example application of labor productivity estimation. Section 5 discusses the implication of our results. Section 6 concludes by highlighting the main findings and providing suggestions.

2 Data and methods

2.1 sWBGT, ESI and Liljegren's model

Here we present the formulas of sWBGT, ESI and Liljegren's model. Parameter definitions and their units within all equations are summarized in the list of notation. sWBGT was developed for heat stress assessment in sports medicine and formulated as (ACSM, 1984):

$$sWBGT = 0.567(T_a - 273.15) + 0.393e_a + 3.94 \tag{1}$$

ESI was designed as an approximation to WBGT via a multiple regression model (D. Moran et al., 2001), and structured as (D. Moran, Pandolf, Shapiro, et al., 2003):

$$ESI = 0.62(T_a - 273.15) - 0.007RH + 0.002S_{down} + 0.0043(T_a - 273.15) \cdot RH - 0.078(0.1 + S_{down})^{-1} \tag{2}$$

Liljegren's model is physically based relying on fundamental principles of heat and mass transfer. It performs energy budget analysis on both natural wet bulb and black globe sensors, which boil down to two separate equations for T_w (eq. 3) and T_g (eq. 5) (Liljegren et al., 2008) that need to be solved by iteration:

$$T_w = T_a - \frac{\Delta H}{c_p}\frac{M_{H2O}}{M_{Air}}(\frac{Pr}{Sc})^{0.56}(\frac{e_w - e_a}{P - e_w}) + \frac{\Delta F_{net}}{Ah} \tag{3}$$

where ΔF_{net} refers to net radiative gain by the wick:

$$\begin{aligned}\Delta F_{net} = \frac{1}{2}\pi DL\epsilon_w(L_{down} + L_{up}) - \pi DL\sigma\epsilon_w T_w^4 + (\pi DL + \frac{\pi D^2}{4})(1 - \alpha_w)(1 - f_{dir})S_{down} \\ + (DL\sin\theta + \frac{\pi D^2}{4}\cos\theta)(1 - \alpha_w)f_{dir}\frac{S_{down}}{\cos\theta} + \pi DL(1 - \alpha_w)S_{up}\end{aligned} \tag{4}$$

$$T_g^4 = \frac{L_{down} + L_{up}}{2\sigma} - \frac{h(T_g - T_a)}{\epsilon_g\sigma} + \frac{S_{down}(1 - \alpha_g)}{2\epsilon_g\sigma}(1 - f_{dir} + \frac{f_{dir}}{2\cos\theta}) + \frac{1 - \alpha_g}{2\epsilon_g\sigma}S_{up} \tag{5}$$

where S_{down}, S_{up}, L_{down} and L_{up} denote surface downward and upwelling solar and longwave radiation respectively. The latter three radiation components were approximated as:

$$L_{down} = \sigma\epsilon_a T_a^4 \tag{6}$$

$$L_{up} = \sigma\epsilon_{sfc}T_{sfc}^4 = \sigma T_a^4 \tag{7}$$

$$S_{up} = \alpha_{sfc} S_{down} \tag{8}$$

In Liljegren's model, air temperature, humidity, wind speed and surface downward solar radiation are required as inputs for solving T_w and T_g. For details of the calculation procedure, please refer to Liljegren et al. (2008). Liljegren's model was originally written in FORTRAN and C-language programs. We rewrote it in Cython language for implementation in Python. Please find the code availability in the Acknowledgement section.

2.2 Bias quantification within an idealized context

Bias distributions of sWBGT and ESI are first identified within an idealized context as a function of four input variables. We apply Liljegren's model in its original form to assessing biases of both metrics across artificially selected ranges of air temperature (20-50°C), relative humidity (5-95%), 2m wind speed (0.13, 0.5, 1.0, 2.0, 3.0m/s), and surface downward solar radiation (0, 300, 500, 700, 900w/m^2). The focus is on conditions under which biases are exceptionally large.

2.3 Bias quantification using ERA5 reanalysis data

With diverse climate regimes spanning across the globe, biases of different magnitudes and/or signs are expected to occur over different regions. It would be useful to reveal the spatial distribution of biases and identify locations where sWBGT/ESI is exceptionally biased and their applications would cause serious under- or over-estimation of heat stress and downstream impacts.

ERA5 reanalysis data (Hersbach, H. et al., 2018; Bell, B. et al., 2020) are used to identify the bias spatial structure in a more realistic setting. Since all four radiation components are available from the ERA5 archive, the approximations in equation 6-8 are no longer necessary. The 2m air and dewpoint temperature, surface pressure, 10m wind speed and surface downward and upwelling solar and thermal radiation on a 0.25°×0.25° grid are used to calculate WBGT at an hourly frequency.

The cosine zenith angle ($\cos\theta$) is needed to project direct solar radiation from a flux through a horizontal plane (as stored in ERA5 reanalysis archive) to a flux through a plane perpendicular to the incoming solar radiation (as required by energy budget analysis) (as denoted by $cos\theta$ term in the denominator within eq. 4-5). Since model radiation components are stored as accumulated-over-time quantities (over each hourly interval in the case of ERA5 reanalysis data), the time average of $cos\theta$ during each interval is needed. However, when the accumulation intervals encompass sunset or sunrise, the inclusion of zeros (when the sun is below the horizon) may make the time average of $\cos\theta$ too small. Being in the denominator, this too small $\cos\theta$ would lead to an overestimation of the projected direct solar radiation and consequently too high WBGT values. A simple approximate solution to this problem is taking the average $\cos\theta$ during only the sunlit part of each interval (please refer to Hogan and Hirahara (2016) or Di Napoli et al. (2020) for the calculation procedure). In Fig. S1, we provide an example of erroneously peaks of WBGT values around sunrise or sunset introduced by using $\cos\theta$ averaged over the whole hourly interval, and also show that the peaks can be removed by averaging $\cos\theta$ only during the sunlit period.

2.4 Labor productivity calculation

Several different labor productivity functions have been applied to assessing heat stress-induced labor reduction (Dunne et al., 2013; Bröde et al., 2018; Kjellstrom et al., 2018; Foster et al., 2021), and here we choose the method adopted by ISO7243 standard for illustrative purposes.

The ISO7243 standard provided WBGT limit reference values ($WBGT_{lim}$) corresponding to the upper limit of the prescriptive zone for different levels of metabolic heat production rates (M in Watts) (ISO, 2017):

$$WBGT_{lim} = 56.7 - 11.5log_{10}(M) + 273.15 \tag{9}$$

For WBGT exceeding the limit value, only a fraction of each hour is allowed for working in order to ensure that the physiological strain during each hour cycle can be recuperated after the rest. This fraction can be used as an estimate of labor productivity (for example, a value of 0.5 indicates a 30min working and 30min rest cycle, and consequently a 50% labor productivity) and calculated as follows (Malchaire, 1979; Bröde et al., 2018):

$$\text{labor productivity} = max\{0; min[1; \frac{WBGT_{lim,rest} - WBGT}{WBGT_{lim,rest} - WBGT_{lim}}]\} \tag{10}$$

2.5 Gridded population dataset

Gridded world population data (GPWv4.11) (Center for International Earth Science Information Network - CIESIN - Columbia University, 2018) with a spatial resolution of 0.25°×0.25° for year 2020 after adjusting to match the country total of United Nations World Population Prospects are employed to calculate global population-weighted labor productivity.

3 Bias quantification

3.1 Idealized setting

In order to understand bias structure and its dependencies on ambient conditions, we calculate sWBGT/ESI biases (sWBGT/ESI - WBGT) across artificially selected ranges of air temperature, relative humidity, wind speed and solar radiation (Fig. 1). In the case of sWBGT, positive biases (sWBGT>WBGT) appear to be dominant, especially during nighttime (zero solar radiation), with bias magnitudes up to more than +10 °C. Nevertheless, negative biases (sWBGT<WBGT) may occur under strong solar radiation and light wind condition. Given any fixed level of solar radiation and wind speed, there tends to be larger positive biases under hotter and more humid condition which is a direct result of sWBGT placing all weights on temperature and humidity.

ESI, in comparison, is mainly subject to negative biases. Wind speed and solar radiation appear to be the dominant factors controlling bias magnitudes with larger negative biases under strong solar radiation and light wind (up to -10 °C under $900 w{\cdot}m^{-2}$ solar radiation and 0.13 m/s wind speed). Under dry condition with relative humidity <10%, ESI exhibits smaller negative biases and even positive ones during nighttime when the bias magnitudes are overall smaller as well.

Although some combinations of the four meteorological inputs shown in figure 1 are physically less plausible (such as large humidity and strong solar radiation), it provides an overall picture of sWBGT/ESI biases across the 4-D climatic space which can serve as a guidance for further detailed bias assessment or practical applications. For example, we expect larger over-estimations by sWBGT during nighttime (or indoor) or under hot-humid climate such as in the tropics, and larger under-estimation by ESI under sunny, calm days. Next, we explore bias structure under the more realistic setting of ERA5 reanalysis data with frequent reference to and comparison with the pattern obtained here.

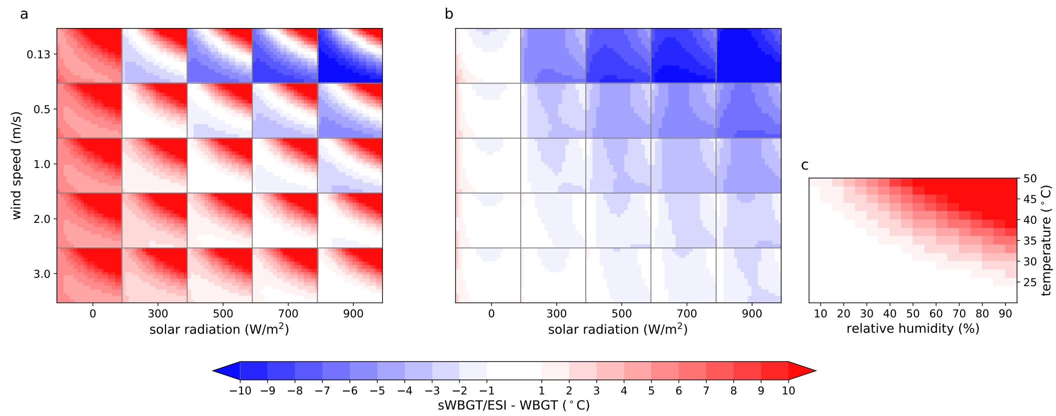

Figure 1. Bias distribution of sWBGT (a) and ESI (b) across an artificial 4-D climatic space of air temperature, relative humidity, 2m wind speed and surface downward solar radiation. Each small box in (a) and (b) depicts bias distribution across a range of temperature (20-50°C) and relative humidity (5-95%) as shown in (c) under fixed levels of solar radiation and wind speed.

3.2 Realistic setting

3.2.1 Biases at climatological mean level

ERA5 reanalysis data are applied to identifying the spatial distribution of biases within a realistic context. First, we assess biases of both metrics in terms of the climatological monthly average (1990-2019) of daily mean, maximum and minimum values (Fig. 2). Since we focus on heat stress, only the hottest calendar month (determined by climatological monthly mean of WBGT) is included. A consistent overestimation by sWBGT is detected across the globe with larger biases for daily minimum (by > 4°C) and smaller biases for daily maximum (Fig. 2e,f). Areas with hot-humid summer, such as the tropics, south Asia, eastern China and southeastern U.S., exhibit larger positive biases (>2°C for daily maximum, >5°C for daily minimum and >4°C for daily mean) (Fig. 2d-f) which is consistent with the bias structure revealed within idealized context (Fig. 1a). Subtropical dry regions show smaller biases in comparison. Additionally, a topography effect is evident with smaller positive or even negative biases for daily maximum over mountainous areas like the Himalayas, Andes, and Rocky Mountains (Fig. 2e), although the WBGT values over these regions are generally small (Fig. 2b).

ESI has smaller overall biases compared with sWBGT. Positive and negative biases within ±1°C occur for daily mean in subtropical dry regions and the tropics respectively (Fig. 2g). Negative biases dominate daily maximum values particularly in the tropics (Fig. 2h). In that region, the bias magnitude is -2 to -3°C due to relatively strong solar radiation and low wind speed over tropical areas as indicated in the idealized results (Fig. 1b). Subtropical dry regions, despite even stronger solar radiation, show smaller negative and even positive biases for daily maximum as a result of low humidity and probably relatively higher wind speed. In the case of daily minimum, the differences between ESI and WBGT are generally small (within ±0.5°C) except over-estimations by 1-2°C over North Africa and Middle East (MENA) dry regions (Fig. 2i). This agrees with the positive biases under dry nighttime conditions revealed within the idealized setting (Fig. 1b).

Compared with sWBGT, ESI appears to be a better approximation particularly for nighttime and daily mean situation. However, the larger negative biases for daily maximum (Fig. 2h) imply that ESI may substantially underestimate daily peak heat stress especially when we turn from climatological mean to individual days or hours.

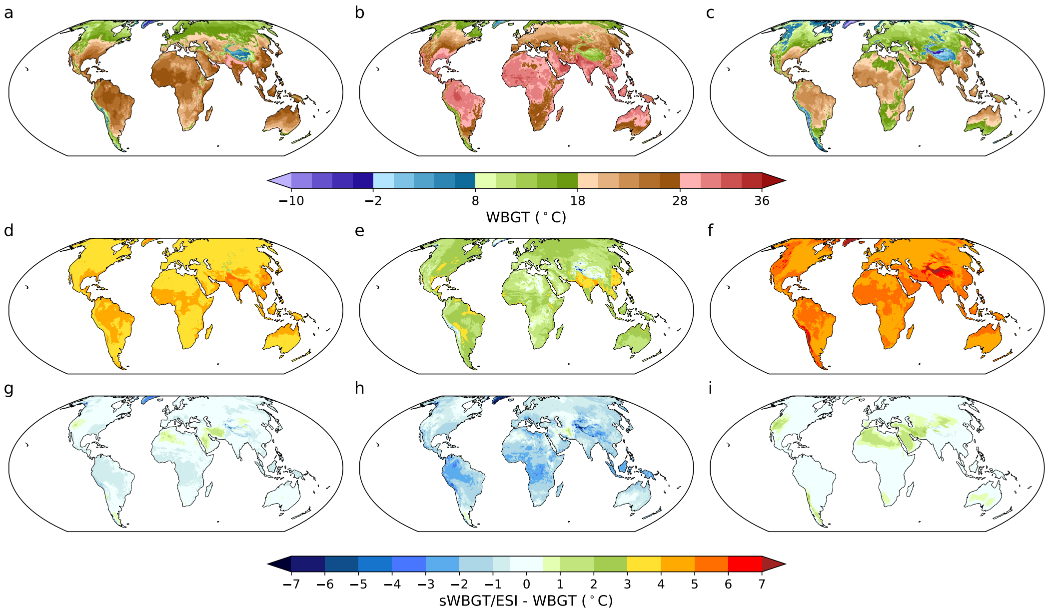

Figure 2. Climatological monthly average (CMA) of daily mean (a), maximum (b) and minimum (c) WBGT for the period 1990-2019. Biases of sWBGT (d-f) and ESI (g-i) with respect to CMA of daily mean (d, g), maximum (e, h) and minimum values (f, i). Only the hottest month (determined by CMA WBGT) being included.

3.2.2 Frequencies of relatively large biases

It bears mentioning that bias quantification in Fig. 2 is based on 30-year climatological means, whereas bias magnitudes can be much larger over certain individual days and/or hours. Here we count the frequencies of relatively large positive and negative biases (beyond ±2°C) based on original hourly time series during 1990-2019 (Fig. 3), with an additional requirement of WBGT exceeding 25°C, the $WBGT_{lim}$ value for very heavy work (a metabolic rate of 520W) according to ISO7243 standard.

sWBGT overestimates WBGT by at least 2°C within more than 30% cases over tropics and other hot-humid area and even more than 80% over the northern part of South Asia (Fig. 3a). In the same region, there are still more than 50% cases even if biases magnitudes are raised to >5°C (Fig. S2). In contrast, underestimations by more than 2°C are rare (<1%) and concentrate in subtropical dry regions presumably under dry, sunny and calm days (Fig. 1a). In the case of ESI, negative biases beyond -2°C are detected for over 10% cases in tropical areas (Fig. 3d); whereas positive biases in ESI by more than 2°C are less frequent and concentrate over west Sahara and Middle East dry regions (<5%) (Fig. 3c).

3.2.3 Biases conditional on WBGT values

It is useful to know whether biases are independent of WBGT values or not. A correlation between them indicates biases of different magnitudes for heat stress of different levels, amongst which the under- or over-estimation of more severe heat stress is of particular concern. To explore it, we calculate and compare biases conditional on the 50th,

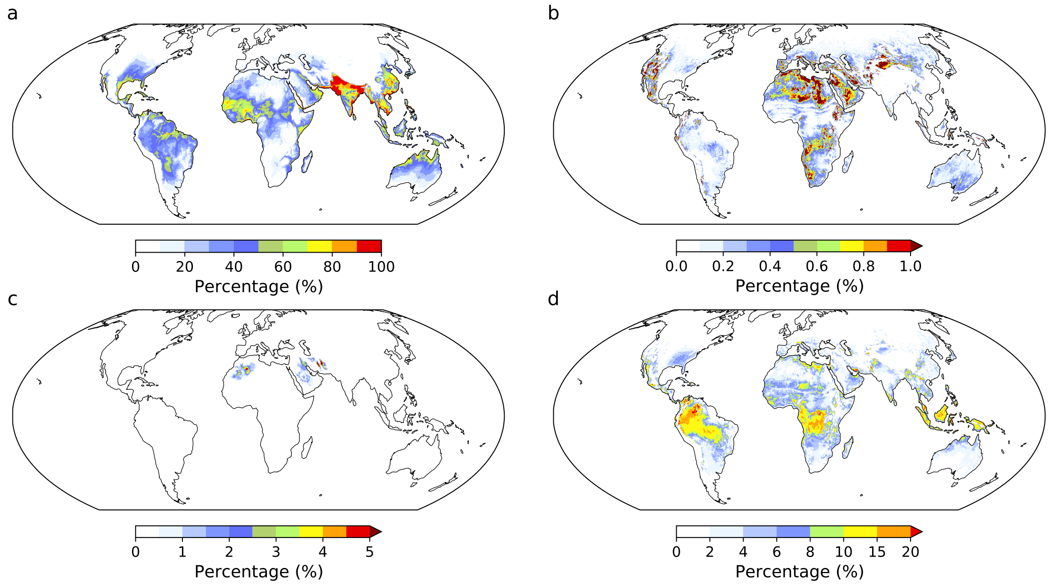

Figure 3. Occurrence percentage of positive (a, c) and negative biases (b, d) larger than ±2°C for sWBGT (a, b) and ESI (c, d) during 1990-2019 with an additional requirement of WBGT exceeding 25°C. Only the hottest month (defined by climatological monthly average WBGT) is included.

75th, 90th, 95th, 99th, and 99.9th percentile exceedance values of WBGT (Fig. 4), which is done for each individual year first and then averaged across the period 1990-2019.

Both sWBGT and ESI show a clear tendency towards smaller positive or stronger negative biases moving from lower to higher percentile exceedance values of WBGT, suggesting a potential correlation between biases and WBGT which is not surprising since both of them are controlled by the same set of meteorological variables (Fig. 1). sWBGT conditional on 50th percentile of WBGT shows substantial positive biases (>3°C globally) which are reduced to <2°C in the majority of the world when conditional on 99th percentile of WBGT. Negative biases even occur in many areas particularly over subtropical dry regions (<-2°C) when we move to 99.9th percentile. ESI exhibits small biases (within ±1°C) worldwide conditional on 50th percentile of WBGT which monotonically shift to strong negative biases conditional on 99.9th percentile of WBGT (<-1°C globally and <-4°C in the low latitudes).

The dependence of biases on WBGT may be explained by the fact that both higher WBGT and stronger negative (or smaller positive) bias tend to be associated with strong solar radiation and light wind (Fig. 1). Based on the results shown here, We expect sWBGT to largely overestimate median-level heat stress but less (or even underestimate) for more severe heat stress (such as the hottest week or 3 days of the year). ESI, in contrast, does a better job in measuring heat stress of median level but tend to seriously underestimate those of more severity.

3.2.4 Biases of extreme values

Extreme events are of special importance in the study of heat stress. For example, some studies attempt to identify extremely rare, short-term events in T_w in the past 30 years and going into the future (Raymond et al., 2020). The stronger negative biases of both metrics conditional on higher percentile exceedance values of WBGT (e.g. Fig.

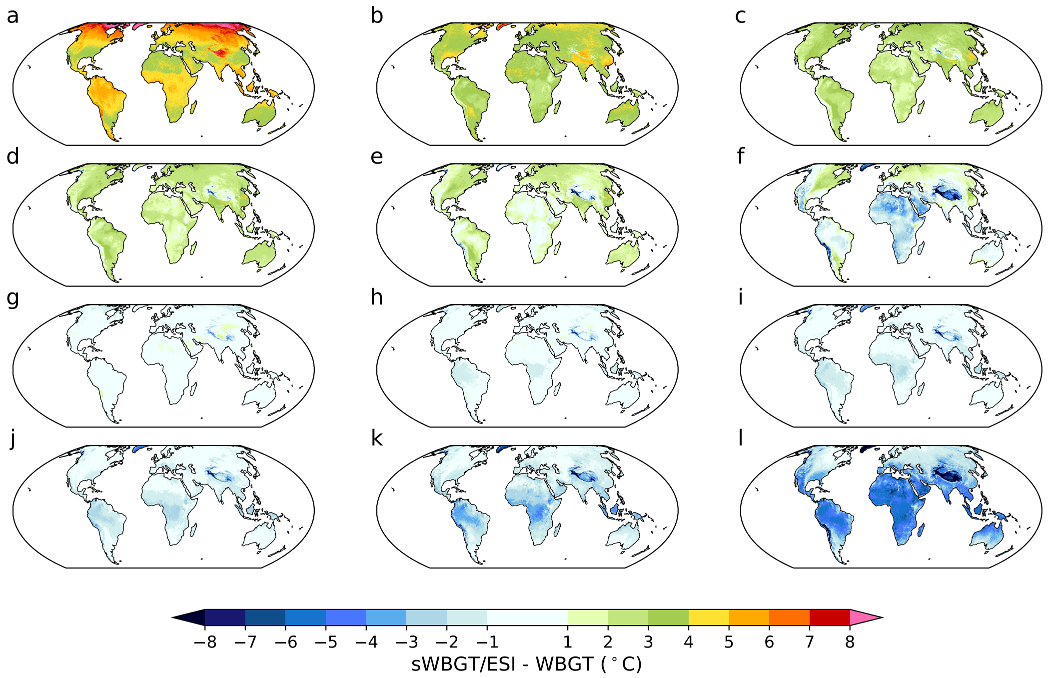

Figure 4. Biases of sWBGT (a-f) and ESI (g-l) conditional on the 50th (a, g), 75th (b, h), 90th (c, i), 95th (d, j), 99th (e, k), and 99.9th (f, l) percentile exceedance values of WBGT during 1990-2019

4f, l) raise a cautionary note that extreme heat stress at some places of the world may be seriously underestimated. Here we implement a generalized extreme value (GEV) analysis to estimate and compare the extreme values of WBGT, sWBGT and ESI at each grid cell. Specifically, a GEV model is fit to the annual maximum (calculated from hourly frequency) of each metric during 1990-2019 using ERA5 reanalysis data. The metric values corresponding to a 1-in-30-year event are calculated and compared (Fig. 5).

Biases of extreme values share similar pattern with those conditional on 99.9 percentile exceedance values of WBGT yet with larger magnitudes. Even in extreme value sWBGT produces overestimated values (by less than 3°C in tropics and other hot-humid area and northern Eurasia, and by 3-5°C in the northeast of North America) in many regions with the notable exception of subtropical dry regions. Large negative biases are detected in MENA region (-4°C to -7°C) (Fig .5d). ESI underestimates WBGT by more than 3°C across most of the world (Fig. 5e). MENA regions stand out with strong negative biases between -6°C and -10°C.

The biases structure of extreme values shown here is not merely a simple extension of patterns observed at climatological mean levels. For example, relatively small biases of ESI at climatological mean level (Fig. 2g-i) suggest it is a potentially acceptable approximation of WBGT for quantifying climatological mean heat stress or its temporal trends. Nevertheless, serious underestimations are expected when it comes to the most extreme heat stress conditions.

3.2.5 Local biases in specific hot-humid and hot-dry regions

It is revealing to explore the bias structure in a more detailed way for two different end-member regimes relevant to heat stress, corresponding to hot-humid and hot-

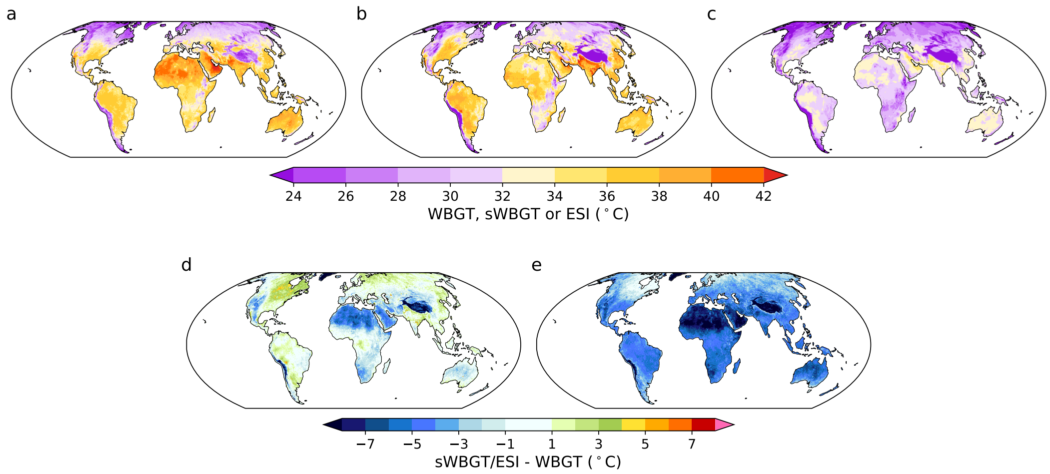

Figure 5. WBGT (a) and ESI (b) return levels corresponding to a 1-in-30-year event, and their differences (ESI-WBGT) (c)

dry climates (Buzan & Huber, 2020). Here Bangladesh and Sahara (Amazon and Arabia) are selected for assessing the bias of sWBGT (ESI). Each region is characterized by a $2^\circ \times 2^\circ$ lat/lon box (Fig. 6).

Biases of sWBGT exhibit similar diurnal cycles at Bangladesh and Sahara with larger positive biases during nighttime and smaller biases during mid-day (Fig. 6a,e) which is consistent with previous studies (Grundstein & Cooper, 2018). sWBGT rarely underestimates WBGT in Bangladesh within hot-humid climate (Fig. 6a-d). Sahara, being hot and dry, sees both positive and negative biases in daytime with the majority of cases being positive biases (Fig. 6e-h). ESI also shows similar diurnal cycles of biases over Amazon and Arabia with smaller biases in nighttime especially for Amazon (Fig. 6i,m). During nighttime in Arabia, ESI consistently overestimates WBGT by around 2°C potentially as a result of low humidity (Fig. 6o).

Consistent with the dependence of biases on WBGT values revealed in Fig. 4, a negative correlation between daytime biases and WBGT values is identified for both metrics (Fig. 6b,f,j,n). This negative correlation indicates a serious underestimation of extreme heat stress by sWBGT at Sahara (up to -10°C for WBGT values above 38°C) and by ESI at both Amazon (around -5°C for WBGT values over 35°C) and Arabia (up to -10°C for WBGT values over 38°C) (Fig. 6f,j,n). The underestimation of extreme heat stress is especially severe at dry regions despite a positive bias at mean level for both metrics. Moreover, solar radiation appears to be negatively (positively) correlated with biases (WBGT) confirming its important role in contributing to the negative correlation between biases and WBGT values. In addition, there is a positive correlation between nighttime biases and WBGT values over Bangladesh (Fig. 6c) probably because both biases and WBGT values are positively correlated with temperature and humidity. This indicates that, when nighttime heat stress is exceptionally severe in hot-humid climate, sWBGT tends to overestimate it even more.

Furthermore, Hot-dry regions have more dispersed bias distribution than hot-humid regions. Bias spread is also much larger during daytime potentially as a result of the large spatial and temporal variability in short-wave radiation.

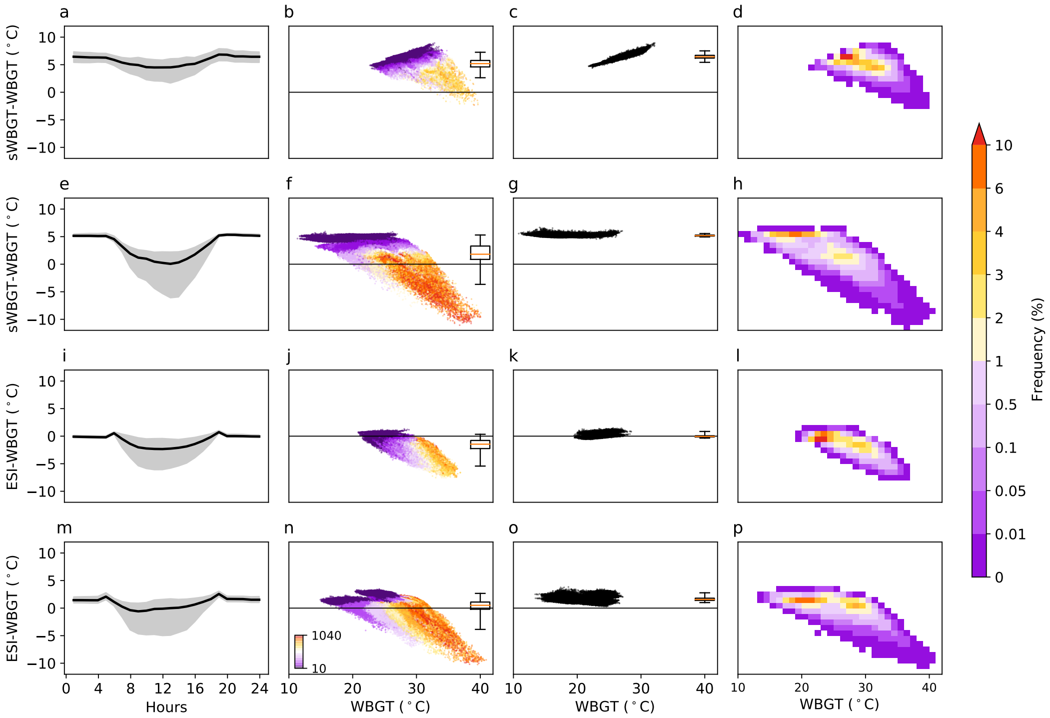

Figure 6. Biases quantification for sWBGT over Bangladesh (23-25°N; 88-90°E) (a-d) and Sahara (22-24°N; 24-26°E) (e-h), and ESI over Amazon (1°S-1°N; 70-72°W) (i-l) and Arabia (25-27°N; 43-45°E) (m-p). The diurnal cycle of biases is plotted in the leftmost column, with the shading area corresponding to 1 to 99th percentiles. Bias scattergrams for daytime and nighttime are plotted in the middle two columns with daytime on the left and nighttime on the right. Boxplots placed within scattergram describe bias spread with box extending from the lower to upper quartile and whiskers representing 1th and 99th percentiles. Daytime scattergram is colored by surface downward solar radiation. Bias frequency heatmap for both daytime and nighttime is plotted in the rightmost column. Data used cover the period 1990-2019 with only the hottest calendar month (defined by climatological monthly average WBGT) included.

4 Application to labor productivity estimation

The sWBGT/ESI biases revealed above are expected to affect the downstream impact assessment of heat stress which might be assessed in many ways depending on the application. Here we take labor productivity estimation as an example to examine the impact of these biases. Labor productivity depends on working intensity measured by metabolic rate. Here we assume a metabolic rate of 415W which is classified as 'high metabolic rate' in ISO7243 standard (ISO, 2017) and representative for agriculture labor. Climatological mean annual labor productivity (1990-2019) is calculated using all three metrics from ERA5 reanalysis data (Fig. 7a-c). sWBGT vastly underestimates labor productivity (as a result of overestimating heat stress) in tropics and other hot-humid areas. The zonal average labor productivity shows large differences across equatorial area with values barely below 90% according to WBGT but as low as 60% as indicated by sWBGT. To put that in context, that bias (30%) is comparable to the labor loss in tropics predicted for a nearly 4.0 degree warming by Buzan and Huber (2020) (Fig. 10 in their paper), and the predicted global labor loss from the beginning to the end of this century under RCP8.5 scenario by Dunne et al. (2013) (Fig. 2 in their paper). ESI clearly did a much better job with respect to deviation magnitudes. It overestimates annual labor productivity by for example 5 percent in tropics (Fig. 7e,f).

In order to take into account population distribution and human exposure, we further calculate population-weighted average annual labor productivity for the globe, tropics and high latitudes during 1950-2019 (Fig. 7g-i). The discrepancy between ESI and WBGT is much smaller and relatively stable along with time leading to similar decreasing trends (-0.26% and -0.33% per decade respectively for global average). However, underestimation of labor productivity by sWBGT became increasingly large resulting in a substantially larger decreasing trends (-1.0% per decade for global average). Namely, positive biases in sWBGT not only cause a serious underestimation of labor productivity but also a substantial exaggeration of labor reduction tendency. This can be explained by the larger positive bias of sWBGT in the hot-humid regime (Fig. 1a). Heat stress overestimation by sWBGT will be further amplified as the world warms with increasing air temperature and only small changes in relative humidity (Byrne & O'Gorman, 2013; Byrne & OGorman, 2018; Buzan & Huber, 2020). In contrast, solar radiation and wind speed, the main controlling factors of ESI bias, have no clear, robust changes with warming over land.

Labor productivity in Fig. 7 is derived by treating both daytime and nighttime hours as potentially available working time. However, people within the majority of industries tend to work in daytime. Some outdoor work (such as field preparation, sowing, and crop harvesting) may rely on daylight making working during nighttime less feasible. Hence, we repeat the labor productivity estimation with only daytime hours included (Fig. S3). The absolute labor productivity is reduced (comparing Fig. S3a-c with Fig. 7a-c). sWBGT still largely underestimate labor productivity (Fig. S3e) although we remove nighttime hours when heat stress is consistently and seriously overestimated by sWBGT (Fig. 1a). Labor productivity overestimation by ESI becomes stronger (Fig. S3f) which is consistent with the tendency of heat stress underestimation by ESI in daytime (Fig. 1b).

Here we estimate annual labor productivity from hourly data which may be not available in most archives such as CMIP and CORDEX. It is common to see studies using sub-daily (de Lima et al., 2021; Buzan & Huber, 2020), daily (Liu, 2020; Altinsoy & Yildirim, 2014; Zhu et al., 2021; Kjellstrom et al., 2018; Orlov et al., 2020) or even monthly output (Dunne et al., 2013) for similar purpose. Although not the focus of this article, it is useful to quantify the potential error introduced thereby. Therefore, the hourly ERA5 reanalysis data are re-sampled to 8 and 4 times daily scale (calculate temporal averages of radiation flux and re-sample instantaneous values of other fields once each 3 and 6 hours interval), and averaged to obtain the daily mean values. The estimation of annual labor productivity (including both daytime and nighttime hours) is then repeated under each temporal resolution (Fig. S4). We found that labor productivity derived from daily average inputs is substantially overestimated especially in the tropics (by around 7 to more than 13 percent) (Fig. S4f), which is not surprising since both WBGT formulation and labor productivity function are nonlinear. Particularly, all existing labor productivity functions involve a lower threshold of WBGT (e.g. 25°C for very heavy work with a metabolic rate of 520W according to ISO7243 standard) below which there is no labor loss. It is likely to have a daily average WBGT below this threshold but much higher WBGT values during peaking daytime hours in which case the labor productivity estimated from daily average WBGT is too optimistic. In terms of population-weighted global and annual average labor productivity, the adoption of daily average inputs introduce a consistent overestimation by around 2.2 percent during the period 1950-2019. Nevertheless, the derived decreasing trend is similar between hourly (-0.33 percent per decade) and daily average inputs (-0.29 percent per decade). In comparison, the 8 or 4 times daily inputs mainly face a sampling issue (despite the time average for radiation fields) which nevertheless only small errors of within ±1 percent in most of the world (Fig. S4b,d).

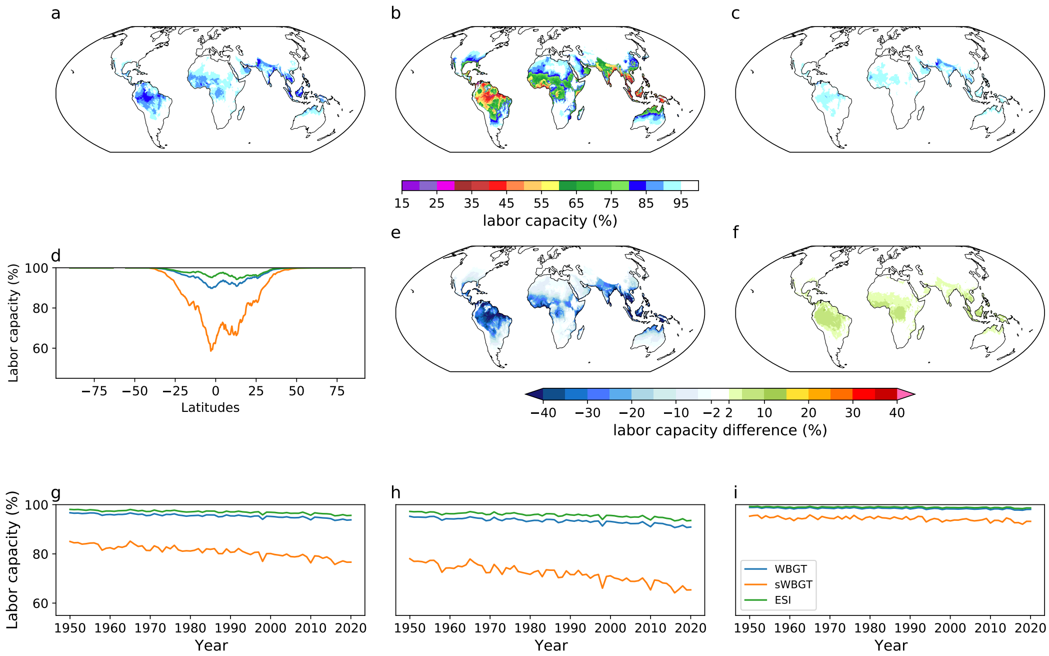

Figure 7. Annual average labor productivity for the period 1990-2019 derived from WBGT (a), sWBGT (b), and ESI (c), with the zonal average value shown in (d). Labor productivity anomaly introduced by using sWBGT (e) and ESI (f). Population weighted annual average labor productivity from 1950 to 2019 across the globe (g), low latitudes (30°S -30°N) (h) and high latitudes (outside of 30°S to 30°N) (i). Labor productivity is quantified assuming a metabolic rate of 415W.

5 Discussion

sWBGT was soundly criticized for missing two ambient factors contributing to heat stress (Budd, 2008). However, it is widely applied because of its simplicity (Smith et al., 2018; Willett & Sherwood, 2010; Kakamu et al., 2017; Cooper et al., 2016; Lee & Min, 2018; Chen et al., 2020; Schwingshackl et al., 2021; Matthews et al., 2017). Particularly, sWBGT has been frequently adopted for estimating heat stress-induced labor productivity reduction both globally (Kjellstrom et al., 2009; Chavaillaz et al., 2019; Knittel et al., 2020) and regionally (Liu, 2020; Altinsoy & Yildirim, 2014; Zhu et al., 2021; Zhang & Shindell, 2021). For instance, under RCP8.5 scenario labor productivity for heavy outdoor work was predicted to decrease by 38% in Southeast Asia and the Middle East by 2050 (Knittel et al., 2020), and more than 40% in South and East China by the end of this century (Liu, 2020); in U.S., around 1.8 billion and 4.4 billion workforce hours were predicted to be lost annually by the 2050s and 2100s under RCP8.5 scenario (Zhang & Shindell, 2021). Such estimates have been applied to informing adaptation strategies (Zhu et al., 2021), or feed into economic models for assessing the downstream socioeconomic impact (Zhang & Shindell, 2021; Chavaillaz et al., 2019; DARA, 2012). However, as we have demonstrated, the adoption of sWBGT may have introduced substantial overestimation of labor and economic loss which may bias the design of greenhouse gas emission policy and decisions of mitigation and/or adaptation investments.

ESI has seen much less applications (de Lima et al., 2021). Its suitability depends more on the application scenarios. The predictions of different heat stress outcomes involve exposure duration of varying lengths and environmental data of different temporal resolutions (Vanos et al., 2020), and hence are affected by biases in varying degrees. For instance, monitoring exertional heatstroke in bricklayers require sub-hourly environment data and will be heavily affected by the serious underestimation of extreme heat stress by ESI during individual peaking hour with high WBGT values. The risk estimation of classic heatstroke generally asks for heat stress information at daily timescale which is then feed into epidemiological models (Vanos et al., 2020). It therefore concerns more about biases at daily mean level. The estimates of labor productivity reduction and the consequent economic impacts typically require heat stress information integrated over a long period such as a year. In this case, ESI may be an acceptable approximation to WBGT due to its relatively small biases under standard climatological conditions.

Many previous studies use daily (Chen et al., 2020; Schwingshackl et al., 2021) or monthly(Newth & Gunasekera, 2018; C. Li et al., 2017; Knutson & Ploshay, 2016; C. Li et al., 2020) average inputs to calculate one of the approximated forms of WBGT, neglecting the fact that WBGT formulation is nonlinear involving nonlinear covariation of temperature and moisture conditions. On one hand, it makes WBGT calculated from temporally averaged inputs overestimated (Buzan et al., 2015); on the other hand, feeding daily or monthly average WBGT into labor response function (Liu, 2020; Altinsoy & Yildirim, 2014; Zhu et al., 2021; Knittel et al., 2020; Zhang & Shindell, 2021; Chavaillaz et al., 2019; Orlov et al., 2020; Dunne et al., 2013) will result in substantial overestimation of labor productivity as we have shown above. For studies using daily average sWBGT to estimate labor productivity (Liu, 2020; Altinsoy & Yildirim, 2014; Zhu et al., 2021; Knittel et al., 2020; Zhang & Shindell, 2021; Chavaillaz et al., 2019), errors introduced by the metrics and the improper time scale may cancel each other to some extent. For the sake of accuracy, it is recommended to use high-temporal-resolution data to calculate heat stress metrics involving the effects of multiple factors such as temperature and humidity. In addition, a heat stress module called HumanIndexMod had been incorporated into the Community Land Model (CLM), the land surface component of the Community Earth System Model (CESM) since CLM4.5 (Buzan et al., 2015). It can enable the calculation of several heat stress metrics (Liljegren's WBGT formulation is not included though) and thermodynamic quantities at each model time step capturing the full nonlinearity of temperature-moisture covariation.

Except sWBGT and ESI, there are also several other approximations to WBGT commonly used within heat stress literature. Orlov et al. (2020) performed a regression analysis against WBGT calculated from Liljegren's formulation and applied the resultant 2nd order polynomial to subsequent calculations. Some studies use the psychrometric wet bulb temperature (T_{pwb}) and air temperature to replace natural wet bulb temperature and black globe temperature leading to the following formula: $WBGT = 0.7* T_{pwb}+0.3*T_a$ (Dunne et al., 2013; Newth & Gunasekera, 2018; C. Li et al., 2017; Knutson & Ploshay, 2016; C. Li et al., 2020; Schwingshackl et al., 2021; D. Li et al., 2020). This simplified form neglects the effects of solar radiation making it only apply to indoor or well-shaded thermal conditions. We find that although the power of Liljegren's formulation has been well recognized 10 years ago (Lemke & Kjellstrom, 2012), it only saw very limited applications (Takakura et al., 2017, 2018; Casanueva et al., 2020; Jacobs et al., 2019; Orlov et al., 2019). One potential reason is that Liljegren's approach is computationally intensive since it requires iterative calculations and careful treatment of latitude, date, and the time of day to get solar radiation correct (Orlov et al., 2020). Moreover, Liljegren's original code was written in C and Fortran language which may be not familiar to most end-users. To tackle this problem, we rewrote the code in Cython which is fast, easy to use in Python and scales well for large dataset. Leveraging on parallel computing enabled by Dask, it takes around half a minute to calculate one-year WBGT at 3-hourly frequency for a GCM with a spatial resolution of $1.5°\times1.5°$ using one node (24 cores) of Brown cluster at Purdue University. We include Liljegren's original formulation as well as the modified version to take advantage of the full set of radiation components in climate model output. Please find the details of code availability in the Acknowledgement section.

6 Summary and conclusions

We explicitly calculated Liljegren's formulation for WBGT and assessed the performance of two previously used, simple approximations WBGT–sWBGT and ESI–against it. The bias structure across the 4-D climatic (atmospheric temperature, shortwave radiation, specific humidity, wind speed) space of this bias was explored within an idealized context. Within this idealized framework, sWBGT is expected to overestimate WBGT during nighttime and under hot-humid days. Both approximate metrics tend to underestimate WBGT within sunny, calm days. An overestimation by ESI may occur under dry nighttime conditions. We also explored the bias distribution driven by ERA5 reanalysis data computed at hourly resolution (from 1990-2019) and find results which are consistent with the structure revealed under idealized context. Under standard climatological conditions, we identify a substantial overestimation by sWBGT across the world and considerably smaller biases for ESI. Nevertheless, biases tend to be negatively correlated with WBGT values suggesting a potentially serious underestimation of most extreme heat stress values by both metrics especially in subtropical dry regions.

Given the large biases of sWBGT, we can not recommend it as a suitable approximation to WBGT, which raises serious questions about prior work, since this is the most commonly used approximation in previous studies. Studies using sWBGT to approximate WBGT need to be reevaluated as likely systematically overestimate heat stress and its impacts over most of the Earth, most of the time, while underestimating the severity of the most extreme (>99.9 percentile exceedance). ESI is more suitable for many applications and it's appropriateness depends more on the application purposes. It may be acceptable for evaluating heat stress at climatological mean level or the integrative downstream impact over a long period (such as annual labor productivity). However, the expected serious underestimation of most extreme heat stress makes it less suitable for epidemiological studies (i.e. on morbidity and mortality), extreme heat stress analysis, or as an operational index for heat warning, heatwave forecasting or guiding activity modification at workplace.

Nevertheless, Liljegren's explicit formulation of WBGT should be preferred over these ad hoc approximations. Our code is straightforward to use and well suited for calculating WBGT from large-size climate model output and reanalysis data.

Notation

$\boldsymbol{c_p}$ specific heat of dry air at constant pressure ($J \cdot kg^1 \cdot K^1$)
$\boldsymbol{D}$ diameter of wick (m)
$\boldsymbol{e_a}$ ambient vapor pressure (hPa)
$\boldsymbol{e_w}$ vapor pressure at the surface of the wick (hPa)
ESI environmental stress index (°C)
$\boldsymbol{f_{dir}}$ fraction of the total horizontal solar irradiance due to the direct beam of the sun
$\boldsymbol{h}$ convective heat transfer coefficient for the wick or black globe ($W \cdot m^{-2} \cdot K^{-1}$))
$\boldsymbol{L}$ length of wick (m)
$\boldsymbol{L_{down}}$ Surface downward long-wave radiation ($W \cdot m^{-2}$)
$\boldsymbol{L_{up}}$ Surface upwellig long-wave radiation ($W \cdot m^{-2}$)
$\boldsymbol{M}$ metabolic heat production rate (W)
$\boldsymbol{M_{Air}}$ molecular weight of dry air (kg)
$\boldsymbol{M_{H2O}}$ molecular weight of water vapor (kg)
$\boldsymbol{RH}$ Relative humidity (%)

$\boldsymbol{Sc}$ Schmidt number
sWBGT simplified wet bulb globe temperature (°C)
$\boldsymbol{S_{down}}$ Surface downward solar radiation ($W \cdot m^{-2}$)
$\boldsymbol{S_{up}}$ Surface upwelling solar radiation ($W \cdot m^{-2}$)
$\boldsymbol{T_a}$ ambient air temperature (K)
$\boldsymbol{T_g}$ Black globe temperature (K)
$\boldsymbol{T_{sfc}}$ surface temperature (K)
$\boldsymbol{T_w}$ natural wet bulb temperature (K)
$\boldsymbol{P}$ surface pressure (hPa)
$\boldsymbol{Pr}$ Prandtl number
$\boldsymbol{WBGT}$ wet bulb globe temperature (K)
$\boldsymbol{WBGT_{lim}}$ WBGT limit reference value (K)
$\boldsymbol{WBGT_{lim,rest}}$ WBGT limit reference value under resting metabolic rate (117 W) (K)
$\boldsymbol{\alpha_g}$ albedo of the globe
$\boldsymbol{\alpha_{sfc}}$ surface albedo
$\boldsymbol{\alpha_w}$ albedo of the wick
$\boldsymbol{\sigma}$ Stefan-Boltzmann constant ($W \cdot m^{-2} \cdot K^{-4}$)
$\boldsymbol{\epsilon_a}$ emissivity of the atmosphere
$\boldsymbol{\epsilon_g}$ globe emissivity
$\boldsymbol{\epsilon_{sfc}}$ surface emissivity
$\boldsymbol{\theta}$ Solar zenith angle (radian)
$\boldsymbol{\Delta F_{net}}$ net radiative gain by the wick from the environment (W)

Acknowledgments

Hersbach, H. et al., (2018) was downloaded from the Copernicus Climate Change Service (C3S) Climate Data Store (`https://cds.climate.copernicus.eu/cdsapp#!/dataset/reanalysis-era5-single-levels?tab=overview`). Bell, B. et al., (2020) was downloaded from the Copernicus Climate Change Service (C3S) Climate Data Store (`https://cds.climate.copernicus.eu/cdsapp#!/dataset/reanalysis-era5-single-levels-preliminary-back-extension?tab=overview`). The results contain modified Copernicus Climate Change Service information 2020. Neither the European Commission nor ECMWF is responsible for any use that may be made of the Copernicus information or data it contains. Center for International Earth Science Information Network - CIESIN - Columbia University (2018) was downloaded from `https://sedac.ciesin.columbia.edu/data/set/gpw-v4-population-count-adjusted-to-2015-unwpp-country-totals-rev11`. Liljegren's WBGT code in C language is accessible at `https://github.com/mdljts/wbgt/blob/master/src/wbgt.c`. Our WBGT code along with a Jupyter notebook introducing its usage are stored within a private repository at Github and will be published and deposited at Zenodo upon the acceptance of this paper. For review purpose, the repository can be temporally viewed at `https://gitfront.io/r/user-1452352/bf213c1f4de06259246d8974f7f16f5be77afc1e/PyWBGT/`. Hosted in the same repository are several other Jupyter notebooks and processed dataset that can be used to reproduce all figures in this paper. A Binder project will be created for this repository once it is published which will enable readers run Jupyter notebooks without installing any packages. Data analyses were performed on Purdue University's high-performance computing cluster using Python (Van Rossum & Drake, 2009) and CDO (Schulzweida, 2019). The following Python packages were utilised: Numpy (Harris et al., 2020), Scipy (Virtanen et al., 2020), Xarray (Hoyer & Hamman, 2017), Dask (Dask Development Team, 2016), Matplotlib (J. D. Hunter, 2007), Cartopy (Met Office, 2010 - 2015), and pyMannKendall (Hussain & Mahmud, 2019). The authors declare no competing interests. This study is Funded by grant NSF 1805808-CBET Innovations at the

Nexus of Food, Energy, and Water Systems (INFEWS: U.S.-China): A multi-scale integrated modeling approach to managing the transition to sustainability and NSF 1829764-OAC CyberTraining: CIU:Cross-disciplinary Training for Findable, Accessible, Interoperable, and Reusable (FAIR) science

References

ABM. (2010). *About the approximation to the WBGT used by the Bureau of Meteorology.* Retrieved 2021-04-03, from `http://www.bom.gov.au/info/thermal_stress/#approximation`

ACSM. (1984). *Position stand on the prevention of thermal injuries during distance running* (Tech. Rep.). Medicine Sci. Sport. Exercise.

Altinsoy, H., & Yildirim, H. A. (2014). Labor productivity losses over western Turkey in the twenty-first century as a result of alteration in WBGT. *Int J Biometeorol*, 9. doi: 10.1007/s00484-014-0863-z

Army, U. (2003). *Heat stress control and heat casualty management* (Tech. Rep.). Technical Bulletin Medical 507/Air Force Pamphlet.

Barriopedro, D., Fischer, E. M., Luterbacher, J., Trigo, R. M., & Garcia-Herrera, R. (2011). The Hot Summer of 2010: Redrawing the Temperature Record Map of Europe. *Science*, *332*(6026), 220–224. doi: 10.1126/science.1201224

Bell, B., Hersbach, H., Berrisford, P., Dahlgren, P., Horányi, A., Muñoz Sabater, J., ... Thépaut, J-N. (2020). ERA5 hourly data on single levels from 1950 to 1978 (preliminary version). *Copernicus Climate Change Service (C3S) Climate Data Store (CDS).* Retrieved 2021-04-05, from `https://cds.climate.copernicus-climate.eu/cdsapp#!/dataset/reanalysis-era5-single-levels-preliminary-back-extension?tab=overview`

Bernard, T. E., & Pourmoghani, M. (1999). Prediction of Workplace Wet Bulb Global Temperature. *Applied Occupational and Environmental Hygiene*, *14*(2), 126–134. doi: 10.1080/104732299303296

Bröde, P., Fiala, D., Lemke, B., & Kjellstrom, T. (2018). Estimated work ability in warm outdoor environments depends on the chosen heat stress assessment metric. *International Journal of Biometeorology*, *62*(3), 331–345. doi: 10.1007/s00484-017-1346-9

Budd, G. M. (2008). Wet-bulb globe temperature (WBGT)–its history and its limitations. *Journal of Science and Medicine in Sport*, *11*(1), 20–32. doi: 10.1016/j.jsams.2007.07.003

Burke, M. B., Miguel, E., Satyanath, S., Dykema, J. A., & Lobell, D. B. (2009). Warming increases the risk of civil war in Africa. *Proceedings of the National Academy of Sciences*, *106*(49), 20670–20674. doi: 10.1073/pnas.0907998106

Buzan, J. R., & Huber, M. (2020). Moist Heat Stress on a Hotter Earth. *Annual Review of Earth and Planetary Sciences*, *48*(1), 623–655. doi: 10.1146/annurev-earth-053018-060100

Buzan, J. R., Oleson, K., & Huber, M. (2015). Implementation and comparison of a suite of heat stress metrics within the Community Land Model version 4.5. *Geoscientific Model Development*, *8*(2), 151–170. doi: 10.5194/gmd-8-151-2015

Byrne, M. P., & O'Gorman, P. A. (2013). Link between landocean warming contrast and surface relative humidities in simulations with coupled climate models. *Geophysical Research Letters*, *40*(19), 5223–5227. doi: 10.1002/grl.50971

Byrne, M. P., & OGorman, P. A. (2018). Trends in continental temperature and humidity directly linked to ocean warming. *Proceedings of the National Academy of Sciences*, *115*(19), 4863–4868. doi: 10.1073/pnas.1722312115

Casanueva, A., Kotlarski, S., Fischer, A. M., Flouris, A. D., Kjellstrom, T., Lemke, B., ... Liniger, M. A. (2020). Escalating environmental summer heat exposurea future threat for the European workforce. *Regional Environmental*

Change, *20*(2), 40. doi: 10.1007/s10113-020-01625-6
Center for International Earth Science Information Network - CIESIN - Columbia University. (2018). *Gridded Population of the World, Version 4 (GPWv4): Population Count Adjusted to Match 2015 Revision of UN WPP Country Totals, Revision 11.* NASA Socioeconomic Data and Applications Center (SEDAC). Retrieved from `https://doi.org/10.7927/H4PN93PB` (Place: Palisades, NY)
Chavaillaz, Y., Roy, P., Partanen, A.-I., Da Silva, L., Bresson, E., Mengis, N., ... Matthews, H. D. (2019). Exposure to excessive heat and impacts on labour productivity linked to cumulative CO2 emissions. *Scientific Reports*, *9*(1), 13711. doi: 10.1038/s41598-019-50047-w
Chen, X., Li, N., Liu, J., Zhang, Z., Liu, Y., & Huang, C. (2020). Changes in Global and Regional Characteristics of Heat Stress Waves in the 21st Century. *Earth's Future*, *8*(11). doi: 10.1029/2020EF001636
Cooper, E. R., Ferrara, M. S., Casa, D. J., Powell, J. W., Broglio, S. P., Resch, J. E., & Courson, R. W. (2016). Exertional Heat Illness in American Football Players: When Is the Risk Greatest? *Journal of Athletic Training*, *51*(8), 593–600. doi: 10.4085/1062-6050-51.8.08
DARA. (2012). *Climate vulnerability monitor: A guide to the cold calculus of a hot planet (2nd ed.)* (Tech. Rep.). Madrid: Fundacion DARA International.
Dask Development Team. (2016). Dask: Library for dynamic task scheduling [Computer software manual]. Retrieved from `https://dask.org`
de Freitas, C. R., & Grigorieva, E. A. (2014). A comprehensive catalogue and classification of human thermal climate indices. *International Journal of Biometeorology*, *59*, 109–120. doi: 10.1007/s00484-014-0819-3
de Lima, C. Z., Buzan, J. R., Moore, F. C., Baldos, U. L. C., Huber, M., & Hertel, T. W. (2021). Heat stress on agricultural workers exacerbates crop impacts of climate change. *Environmental Research Letters*, *16*(4), 044020. doi: 10.1088/1748-9326/abeb9f
Dernedde, E., & Gilbert, D. (1991). Predicction of Wet-Bulb Globe Temperatures in aluminum smelters. *American Industrial Hygiene Association Journal*, *52*(3), 120–126. doi: 10.1080/15298669191364451
Diffenbaugh, N. S., & Giorgi, F. (2012). Climate change hotspots in the CMIP5 global climate model ensemble. *Climatic Change*, *114*(3-4), 813–822. doi: https://doi.org/10.1007/s10584-012-0570-x
Di Napoli, C., Hogan, R. J., & Pappenberger, F. (2020). Mean radiant temperature from global-scale numerical weather prediction models. *International Journal of Biometeorology*, *64*(7), 1233–1245. doi: 10.1007/s00484-020-01900-5
Dunne, J. P., Stouffer, R. J., & John, J. G. (2013). Reductions in labour capacity from heat stress under climate warming. *Nature Climate Change*, *3*(6), 563–566. doi: 10.1038/nclimate1827
Ebi, K. L., Vanos, J., Baldwin, J. W., Bell, J. E., Hondula, D. M., Errett, N. A., ... Berry, P. (2021). Extreme Weather and Climate Change: Population Health and Health System Implications. *Annual Review of Public Health*, *42*(1), 293–315. doi: 10.1146/annurev-publhealth-012420-105026
Epstein, Y., & Moran, D. S. (2006). Thermal Comfort and the Heat Stress Indices. *Industrial Health*, *44*(3), 388–398. doi: 10.2486/indhealth.44.388
Foster, J., Smallcombe, J. W., Hodder, S., Jay, O., Flouris, A. D., Nybo, L., & Havenith, G. (2021). An advanced empirical model for quantifying the impact of heat and climate change on human physical work capacity. *International Journal of Biometeorology*, *65*(7), 1215–1229. doi: 10.1007/s00484-021-02105-0
Gaspar, A. R., & Quintela, D. A. (2009). Physical modelling of globe and natural wet bulb temperatures to predict WBGT heat stress index in outdoor environments. *International Journal of Biometeorology*, *53*(3), 221–230. doi:

10.1007/s00484-009-0207-6

Grundstein, A., & Cooper, E. (2018). Assessment of the Australian Bureau of Meteorology wet bulb globe temperature model using weather station data. *International Journal of Biometeorology*, *62*(12), 2205–2213. doi: 10 .1007/s00484 -018-1624-1

Harris, C. R., Millman, K. J., van der Walt, S. J., Gommers, R., Virtanen, P., Cournapeau, D., . . . Oliphant, T. E. (2020). Array programming with NumPy. *Nature*, *585*(7825), 357–362. doi: 10.1038/s41586-020-2649-2

Havenith, G., & Fiala, D. (2015). Thermal Indices and Thermophysiological Modeling for Heat Stress. In R. Terjung (Ed.), *Comprehensive Physiology* (pp. 255–302). Hoboken, NJ, USA: John Wiley & Sons, Inc. doi: 10.1002/cphy.c140051

Hersbach, H., Bell, B., Berrisford, P., Biavati, G., Horányi, A., Muñoz Sabater, J., . . . Thépaut, J-N. (2018). ERA5 hourly data on single levels from 1979 to present. *Copernicus Climate Change Service (C3S) Climate Data Store (CDS)*. doi: 10.24381/cds.adbb2d47

Hogan, R. J., & Hirahara, S. (2016). Effect of solar zenith angle specification in models on mean shortwave fluxes and stratospheric temperatures. *Geophysical Research Letters*, *43*(1), 482–488. doi: 10.1002/2015GL066868

Hoyer, S., & Hamman, J. (2017). xarray: N-D labeled arrays and datasets in Python. *Journal of Open Research Software*, *5*(1). doi: 10.5334/jors.148

Hsiang, S., Kopp, R., Jina, A., Rising, J., Delgado, M., Mohan, S., . . . Houser, T. (2017). Estimating economic damage from climate change in the United States. *Science*, *356*(6345), 1362–1369. doi: 10.1126/science.aal4369

Hunter, C. H., & Minyard, C. O. (1999). *Estimating wet bulb globe temperature using standard meteorological measurements* (Tech. Rep. No. WSRC-MS-9900757). Aiken: Westinghouse Savannah River Company.

Hunter, J. D. (2007). Matplotlib: A 2d graphics environment. *Computing in Science & Engineering*, *9*(3), 90–95. doi: 10.1109/MCSE.2007.55

Hussain, M. M., & Mahmud, I. (2019). pymannkendall: a python package for non parametric mann kendall family of trend tests. *Journal of Open Source Software*, *4*(39), 1556. doi: 10.21105/joss.01556

ISO. (2017). *Ergonomics of the thermal environment Assessment of heat stress using the WBGT (wet bulb globe temperature) index* (International Standard). Geneva: International Organization for Standardization (ISO).

Jacobs, C., Singh, T., Gorti, G., Iftikhar, U., Saeed, S., Syed, A., . . . Siderius, C. (2019). Patterns of outdoor exposure to heat in three South Asian cities. *Science of the Total Environment*, *674*, 264–278. doi: 10 .1016 / j.scitotenv.2019.04.087

Kakamu, T., Wada, K., Smith, D. R., Endo, S., & Fukushima, T. (2017). Preventing heat illness in the anticipated hot climate of the Tokyo 2020 Summer Olympic Games. *Environmental Health and Preventive Medicine*, *22*(1), 68. doi: 10.1186/s12199-017-0675-y

Kjellstrom, T., Briggs, D., Freyberg, C., Lemke, B., Otto, M., & Hyatt, O. (2016). Heat, Human Performance, and Occupational Health: A Key Issue for the Assessment of Global Climate Change Impacts. *Annual Review of Public Health*, *37*(1), 97–112. doi: 10.1146/annurev-publhealth-032315-021740

Kjellstrom, T., Freyberg, C., Lemke, B., Otto, M., & Briggs, D. (2018). Estimating population heat exposure and impacts on working people in conjunction with climate change. *International Journal of Biometeorology*, *62*(3), 291–306. doi: 10.1007/s00484-017-1407-0

Kjellstrom, T., Kovats, R. S., Lloyd, S. J., Holt, T., & Tol, R. S. J. (2009). The Direct Impact of Climate Change on Regional Labor Productivity. *Archives of Environmental & Occupational Health*, *64*(4), 217–227. doi: 10.1080/19338240903352776

Knittel, N., Jury, M. W., Bednar-Friedl, B., Bachner, G., & Steiner, A. K. (2020). A global analysis of heat-related labour productivity losses under climate changeimplications for Germanys foreign trade. *Climatic Change*, *160*(2), 251–269. doi: 10.1007/s10584-020-02661-1

Knutson, T. R., & Ploshay, J. J. (2016). Detection of anthropogenic influence on a summertime heat stress index. *Climatic Change*, *138*(1-2), 25–39. doi: 10.1007/s10584-016-1708-z

Lee, S.-M., & Min, S.-K. (2018). Heat Stress Changes over East Asia under 1.5 and 2.0C Global Warming Targets. *Journal of Climate*, *31*(7), 2819–2831. doi: 10.1175/JCLI-D-17-0449.1

Lemke, B., & Kjellstrom, T. (2012). Calculating workplace WBGT from meteorological data: a tool for climate change assessment. *Industrial Health*, *50*(4), 267–278. doi: 10.2486/indhealth.MS1352

Li, C., Sun, Y., Zwiers, F., Wang, D., Zhang, X., Chen, G., & Wu, H. (2020). Rapid Warming in Summer Wet Bulb Globe Temperature in China with Human-Induced Climate Change. *Journal of Climate*, *33*(13), 5697–5711. doi: 10.1175/JCLI-D-19-0492.1

Li, C., Zhang, X., Zwiers, F., Fang, Y., & Michalak, A. M. (2017). Recent Very Hot Summers in Northern Hemispheric Land Areas Measured by Wet Bulb Globe Temperature Will Be the Norm Within 20 Years. *Earth's Future*, *5*(12), 1203–1216. doi: 10.1002/2017EF000639

Li, D., Yuan, J., & Kopp, R. E. (2020). Escalating global exposure to compound heat-humidity extremes with warming. *Environmental Research Letters*, *15*(6), 064003. doi: 10.1088/1748-9326/ab7d04

Liljegren, J. C., Carhart, R. A., Lawday, P., Tschopp, S., & Sharp, R. (2008). Modeling the Wet Bulb Globe Temperature Using Standard Meteorological Measurements. *Journal of Occupational and Environmental Hygiene*, *5*(10), 645–655. doi: 10.1080/15459620802310770

Liu, X. (2020). Reductions in Labor Capacity from Intensified Heat Stress in China under Future Climate Change. *International Journal of Environmental Research and Public Health*, *17*(4), 1278. doi: 10.3390/ijerph17041278

Maia-Silva, D., Kumar, R., & Nateghi, R. (2020). The critical role of humidity in modeling summer electricity demand across the United States. *Nature Communications*, *11*(1), 1686. doi: 10.1038/s41467-020-15393-8

Malchaire, J. (1979). The TLV workrest regimens for occupational exposure to heat: a review of their development. *The Annals of Occupational Hygiene*, *22*(1), 55–62. doi: 10.1093/annhyg/22.1.55

Masuda, Y. J., Garg, T., Anggraeni, I., Ebi, K., Krenz, J., Game, E. T., ... Spector, J. T. (2021). Warming from tropical deforestation reduces worker productivity in rural communities. *Nature Communications*, *12*(1), 1601. doi: 10.1038/s41467-021-21779-z

Matthews, T. K. R., Wilby, R. L., & Murphy, C. (2017). Communicating the deadly consequences of global warming for human heat stress. *Proceedings of the National Academy of Sciences*, *114*(15), 3861–3866. doi: 10.1073/pnas.1617526114

Meehl, G. A., & Tebaldi, C. (2004). More intense, more frequent, and longer lasting heat waves in the 21st century. *Science*, *305*(5686), 994–997. doi: 10.1126/science.1098704

Met Office. (2010 - 2015). Cartopy: a cartographic python library with a matplotlib interface [Computer software manual]. Exeter, Devon. Retrieved from `https://scitools.org.uk/cartopy`

Mora, C., Counsell, C. W., Bielecki, C. R., & Louis, L. V. (2017). Twenty-Seven Ways a Heat Wave Can Kill You:: Deadly Heat in the Era of Climate Change. *Circulation: Cardiovascular Quality and Outcomes*, *10*(11). doi: 10.1161/CIRCOUTCOMES.117.004233

Moran, D., Pandolf, K., Heled, Y., & Gonzalez, R. (2004). Evaluation of the environmental stress index (ESI) for different terrestrial elevations below and above sea level. *Journal of Thermal Biology*, *29*(6), 291–297. doi: 10.1016/j.jtherbio.2004.05.007

Moran, D., Pandolf, K., Laor, A., Heled, Y., Matthew, W., & Gonzalez, R. (2003). Evaluation and Refinement of the Environmental Stress Index for Different Climatic Conditions. *Journal of Basic and Clinical Physiology and Pharmacology*, *14*(1), 1–16. doi: 10.1515/JBCPP.2003.14.1.1

Moran, D., Pandolf, K., Shapiro, Y., Heled, Y., Shani, Y., Mathew, W. T., & Gonzalez, R. R. (2001). An environmental stress index (ESI) as a substitute for the wet bulb globe temperature (WBGT). *Journal of Thermal Biology*, *26*(4), 427–431. doi: 10.1016/S0306-4565(01)00055-9

Moran, D., Pandolf, K., Shapiro, Y., Laor, A., Heled, Y., & Gonzalez, R. (2003). Evaluation of the environmental stress index for physiological variables. *Journal of Thermal Biology*, *28*(1), 43–49. doi: 10.1016/S0306-4565(02)00035-9

Moran, D. S., Pandolf, K. B., Epstein, Y., Heled, Y., Shapiro, Y., & Gonzalez, R. R. (2005). Validation of the environmental stress index (ESI) for physiological variables. In *Elsevier Ergonomics Book Series* (Vol. 3, pp. 495–501). Elsevier. doi: 10.1016/S1572-347X(05)80077-1

Moran, D. S., Pandolf, K. B., Vitalis, A., Heled, Y., Parker, R., & Gonzalez, R. R. (2004). Evaluation of the environmental stress index (ESI) for the southern hemisphere. *Journal of Thermal Biology*, *29*(7-8), 535–538. doi: 10.1016/j.jtherbio.2004.08.025

Newth, D., & Gunasekera, D. (2018). Projected Changes in Wet-Bulb Globe Temperature under Alternative Climate Scenarios. *Atmosphere*, *9*(5), 187. doi: 10.3390/atmos9050187

NIOSH. (2016). *Criteria for a Recommended Standard: Occupational Exposure to Heat and Hot Environments* (Tech. Rep. No. DHHS (NIOSH) Publication No. 2016-106). Washington, D.C: DHHS, NIOSH.

Orlov, A., Sillmann, J., Aaheim, A., Aunan, K., & de Bruin, K. (2019). Economic Losses of Heat-Induced Reductions in Outdoor Worker Productivity: a Case Study of Europe. *Economics of Disasters and Climate Change*, *3*(3), 191–211. doi: 10.1007/s41885-019-00044-0

Orlov, A., Sillmann, J., Aunan, K., Kjellstrom, T., & Aaheim, A. (2020). Economic costs of heat-induced reductions in worker productivity due to global warming. *Global Environmental Change*, *63*, 102087. doi: 10.1016/j.gloenvcha.2020.102087

Raymond, C., Matthews, T., & Horton, R. M. (2020). The emergence of heat and humidity too severe for human tolerance. *Science Advances*, *6*(19), eaaw1838. doi: 10.1126/sciadv.aaw1838

Schleussner, C.-F., Donges, J. F., Donner, R. V., & Schellnhuber, H. J. (2016). Armed-conflict risks enhanced by climate-related disasters in ethnically fractionalized countries. *Proceedings of the National Academy of Sciences*, *113*(33), 9216–9221. doi: 10.1073/pnas.1601611113

Schulzweida, U. (2019). *Cdo user guide.* doi: 10.5281/zenodo.3539275

Schwingshackl, C., Sillmann, J., VicedoCabrera, A. M., Sandstad, M., & Aunan, K. (2021). Heat Stress Indicators in CMIP6: Estimating Future Trends and Exceedances of ImpactRelevant Thresholds. *Earth's Future*, *9*(3). doi: 10.1029/2020EF001885

Shen, B., Hu, X., & Wu, H. (2020). Impacts of climate variations on crime rates in Beijing, China. *Science of The Total Environment*, *725*, 138190. doi: 10.1016/j.scitotenv.2020.138190

Sherwood, S. C., & Huber, M. (2010). An adaptability limit to climate change due to heat stress. *Proceedings of the National Academy of Sciences*, *107*(21), 9552–9555. doi: 10.1073/pnas.0913352107

Smith, M. T., Reid, M., Kovalchik, S., Woods, T. O., & Duffield, R. (2018). Heat stress incident prevalence and tennis matchplay performance at the Australian Open. *Journal of Science and Medicine in Sport*, *21*(5), 467–472. doi: 10.1016/j.jsams.2017.08.019

Takakura, J., Fujimori, S., Takahashi, K., Hasegawa, T., Honda, Y., Hanasaki, N., ... Masui, T. (2018). Limited Role of Working Time Shift in Offsetting the Increasing OccupationalHealth Cost of Heat Exposure. *Earth's Future*, *6*(11), 1588–1602. doi: 10.1029/2018EF000883

Takakura, J., Fujimori, S., Takahashi, K., Hijioka, Y., Hasegawa, T., Honda, Y., & Masui, T. (2017). Cost of preventing workplace heat-related illness through worker breaks and the benefit of climate-change mitigation. *Environmental Research Letters*, *12*(6), 064010. doi: 10.1088/1748-9326/aa72cc

Vanos, J. K., Baldwin, J. W., Jay, O., & Ebi, K. L. (2020). Simplicity lacks robustness when projecting heat-health outcomes in a changing climate. *Nature Communications*, *11*(1), 6079. doi: 10.1038/s41467-020-19994-1

Van Rossum, G., & Drake, F. L. (2009). *Python 3 reference manual*. Scotts Valley, CA: CreateSpace.

Virtanen, P., Gommers, R., Oliphant, T. E., Haberland, M., Reddy, T., Cournapeau, D., ... SciPy 1.0 Contributors (2020). SciPy 1.0: Fundamental Algorithms for Scientific Computing in Python. *Nature Methods*, *17*, 261–272. doi: 10.1038/s41592-019-0686-2

Willett, K. M., & Sherwood, S. (2010). Exceedance of heat index thresholds for 15 regions under a warming climate using the wet-bulb globe temperature. *International journal of climatology*, *32*(2), 161–177. doi: 10.1002/joc.2257

Yaglou, C. P., & Minard, D. (1957). Control of heat casualties at military training centers. *A.M.A. archives of industrial health*, *16*(4), 302–316.

Zhang, Y., & Shindell, D. T. (2021). Costs from labor losses due to extreme heat in the USA attributable to climate change. *Climatic Change*, *164*(3-4), 35. doi: 10.1007/s10584-021-03014-2

Zhu, J., Wang, S., Zhang, B., & Wang, D. (2021). Adapting to Changing Labor Productivity as a Result of Intensified Heat Stress in a Changing Climate. *GeoHealth*, *5*(4). doi: 10.1029/2020GH000313

Supporting Information for "Explicit calculations of Wet Bulb Globe Temperature compared with approximations and why it matters for labor productivity"

Qinqin Kong[1]and Matthew Huber[1]

[1]Department of Earth, Atmospheric, and Planetary Sciences, Purdue University, West Lafayette, United States of America, 47907

Contents of this file

1. Figures S1 to S4

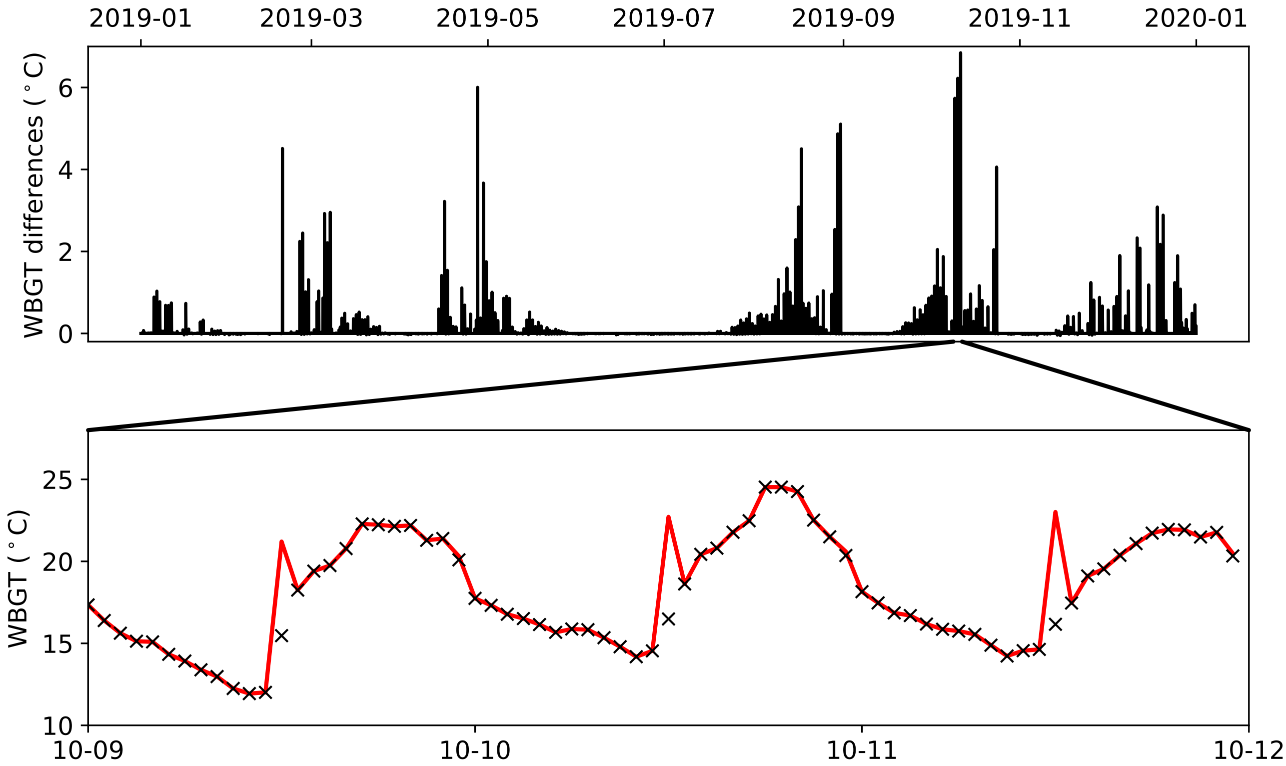

Figure S1. Comparison between WBGTs calculated with the average cosine zenith angle during each hourly interval ($\overline{cos\theta}$) and that during only the sunlit part of each interval ($\overline{cos\theta_{sunlit}}$). A grid cell at 36°N and 84.25°E (close to Y-12 National Security Complex in U.S.) is selected for demonstration purpose. Shown in upper panel are differences in hourly WBGT values calculated from two types of cosine zenith angle in 2019 (WBGT calculated from $\overline{cos\theta}$ - WBGT calculated from $\overline{cos\theta_{sunlit}}$). The lower panel zooms in a 3-day period from October 9 to 11, 2019 showing WBGTs calculated with $\overline{cos\theta}$ (red solid curve) and $\overline{cos\theta_{sunlit}}$ (black cross). WBGT values calculated from $\overline{cos\theta}$ show erroneous peaks around sunrise.

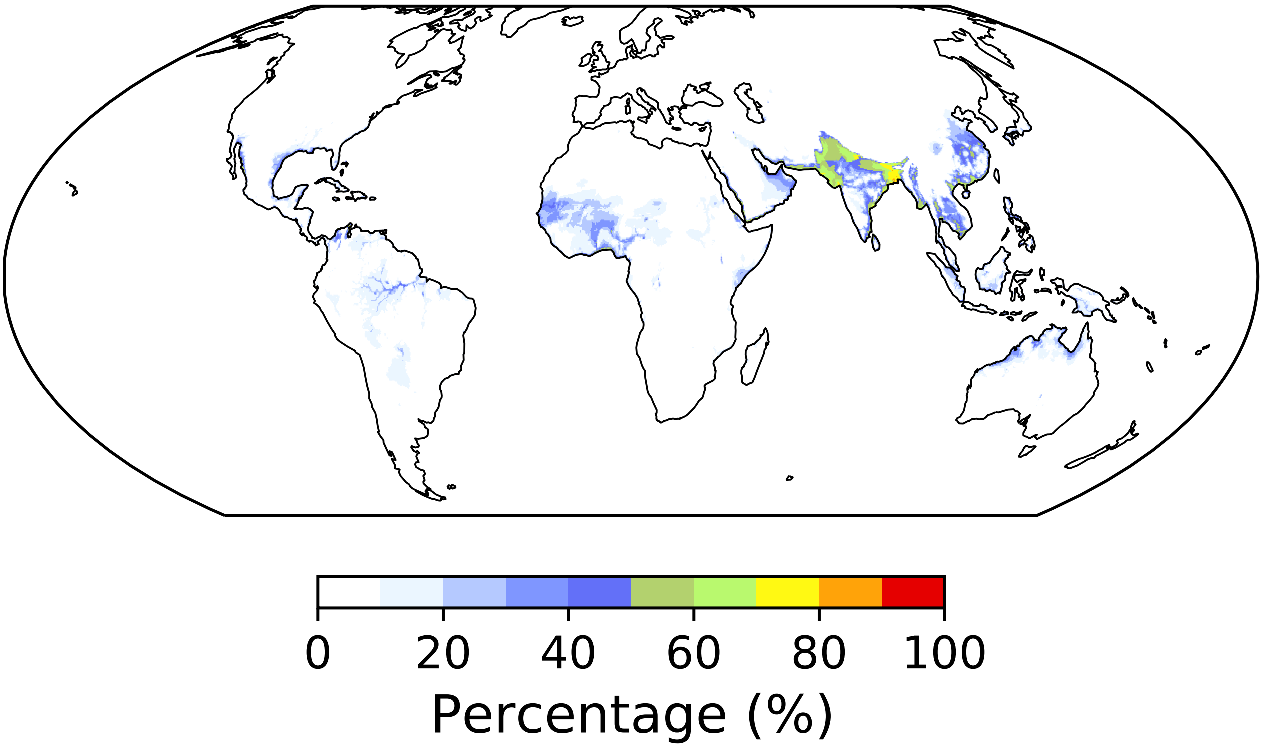

Figure S2. Occurrence percentage of positive biases >5°C for sWBGT during 1990-2019 with an additional requirement of WBGT >= 25°C. Only the hottest calendar month (defined by climatological monthly average WBGT) is included.

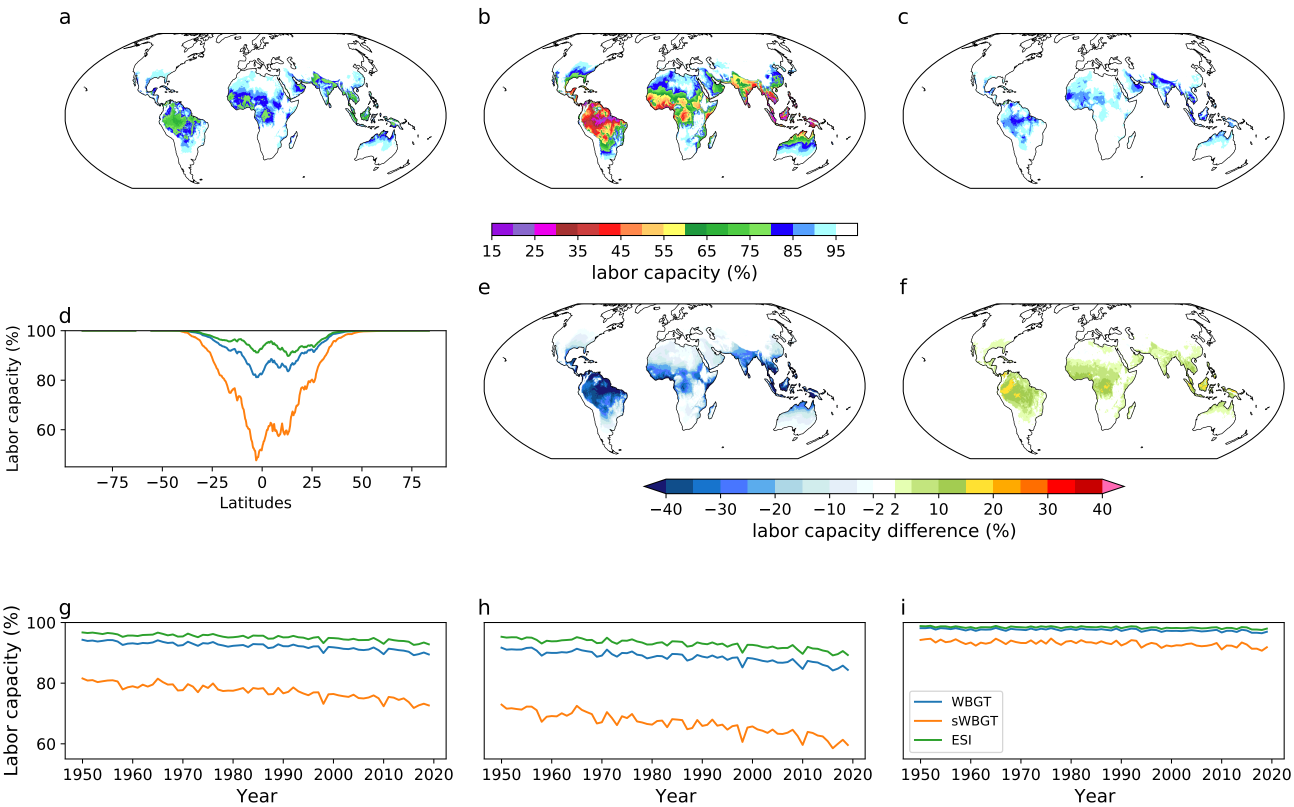

Figure S3. Same as Fig. 7 but labor capacity is calculated during daytime only

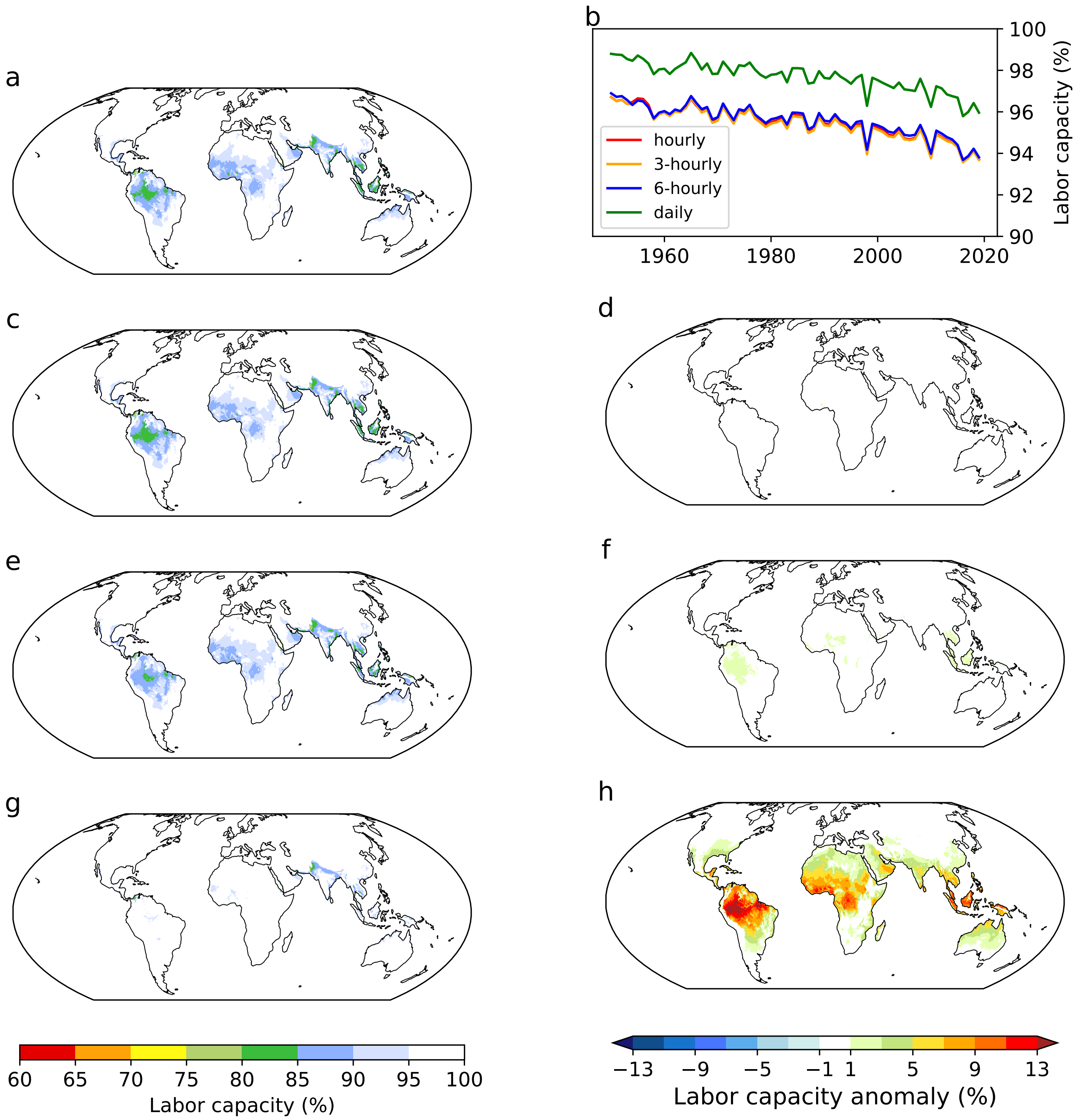

Figure S4. Annual average labor productivity calculated from hourly inputs (a); annual average labor productivity calculated from 8 times daily (c), 4 times daily (e), and daily average inputs (g), and their anomalies (d, f, h respectively) compared with that based on hourly inputs (other resolutions minus hourly); population weighted global annual average labor productivity during 1950-2019 (b).